ACS APPLIED MATERIALS & INTERFACES

Research Article

www.acsami.org

Controlling Conjugation and Solubility of Donor–Acceptor Semiconducting Copolymers for High-Performance Organic Field-Effect Transistors

Mi Jang,[†] Ji-Hoon Kim,[‡] Do-Hoon Hwang,*[,‡] and Hoichang Yang*[,†]

[†]Department of Applied Organic Materials Engineering, Inha University, Incheon 402-751, Korea

[‡]Department of Chemistry, Chemistry Institute for Functional Materials, Pusan National University, Busan 609-735, Korea

Supporting Information

ABSTRACT: Diketopyrrolopyrrole (DPP)-based copolymers, including poly[2,5-bis(2-octyldodecyl)pyrrolo[3,4-*c*]-pyrrole-1,4(2*H*,5*H*)-dione-(*E*)-1,2-di([2,2′-bithiophen]-5-yl)-ethene] (PDDBE) and poly[2,5-bis(2-octyldodecyl)pyrrolo-[3,4-*c*]pyrrole-1,4(2*H*,5*H*)-dione-(*E*)-1,2-bis(6-hexylthieno-[3,2-*b*]thiophen-2-yl)ethene] (PDTTE), were synthesized by alternating a DPP-derivative acceptor (A) block with different donor (D) blocks, such as (*E*)-1,2-di([2,2′-bithiophen]-5-yl)ethene (DBE) and (*E*)-1,2-bis(6-hexylthieno[3,2-*b*]-thiophen-2-yl)ethene (TTE). As solution-processed semiconducting channel layers in organic field-effect transistors (OFETs), PDDBE and PDTTE copolymers had drastically different ordered structures on polymer-grafted SiO_2 dielectrics. Multiple-layered domains of PDDBE had a long-range, π-conjugated extension but a wide π-stacking distance, $d_{(010)}$, of 3.90 Å. One-dimensional nanorod-percolated agglomerates of PDTTE had a much shorter $d_{(010)}$ of 3.71 Å, originating from the alternating A–D structures of the DPP derivative with different D blocks. The corresponding ordered domains yielded a wide range of field-effect mobilities from 0.01 to 1.40 $cm^2\ V^{-1}\ s^{-1}$ in the OFETs.

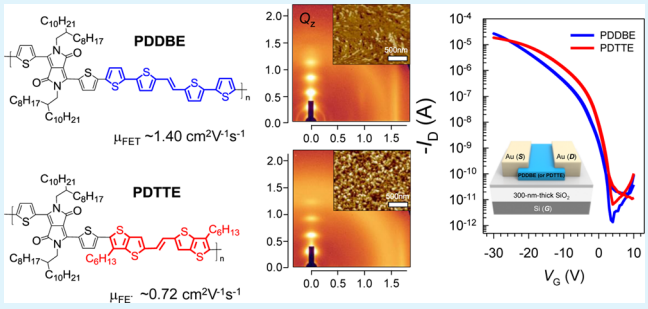

KEYWORDS: *diketopyrrolopyrrole, donor–acceptor, layered conjugation, semiconducting polymer, field-effect transistor*

1. INTRODUCTION

Semiconducting polymers have potential advantages for use in solution-processable and low-cost electronics such as displays,[1,2] radio frequency identification tags,[3,4] organic photovoltaics,[5,6] and sensors.[7,8] As a core component in these electronics, organic field-effect transistors (OFETs) have achieved and exceeded the electrical performance of conventional amorphous-silicon-based FETs, with field-effect mobilities (μ_{FET}) above 1 $cm^2\ V^{-1}\ s^{-1}$.[9−11] Significant improvement has been possible by using solution-processable semiconducting oligomers, which can form large-scale, π-conjugated crystal structures.[11,12] However, the substrate-susceptible crystal growth and fragile crystal characteristics of these oligomers do not make them deformable for flexible electronic applications. In contrast, polymeric semiconductors have reliable solution processability and are mechanically robust but tend to grow into ordered nanofibrillar networks in solution-processed films, giving them relatively poor electrical properties for OFETs.[13,14]

A popular recent synthetic approach for low band gap polymers is to alternate blocks of an electron-deficient (acceptor, A) group and an electron-rich (donor, D) group within the conjugated chain.[10,15,16] Although a large number of A–D copolymers have been studied, diketopyrrolopyrrole (DPP)-based copolymers have attracted extensive attention in organic electronics, because the DPP derivatives can be synthesized simply and have excellent electrical properties.[5,6] By alternating a specific D block at the 2- and 5-positions of the DPP derivative, the resulting copolymers can have huge differences in delocalized π-conjugated energy state, solubility, and self-assembly, yielding different electrical properties.[5,17,18] Many DPP-based copolymers have competed with high-mobility semiconductors, as materials for commercially feasible organic electronics.[5,10,19]

Due to the strong interaction between the conjugated planar backbones of DPP-based copolymers, long alkyl side-chains have been introduced to enhance solution-based film fabrication, although these side-chains often interfere with both intra- and inter-molecular self-assembly. Therefore, the delocalized energy state and processability of the π-conjugated DPP-based copolymers must be optimized for large-scale, solution-based OFET applications.

Here, we synthesized DPP-based copolymers with different D blocks (Scheme 1): poly[2,5-bis(2-octyldodecyl)pyrrolo[3,4-*c*]pyrrole-1,4(2*H*,5*H*)-dione-(*E*)-1,2-di([2,2′-bithiophen]-5-yl)-ethene] (PDDBE) and poly[2,5-bis(2-octyldodecyl)pyrrolo-

Received: February 25, 2015
Accepted: May 27, 2015
Published: May 27, 2015

DOI: 10.1021/acsami.5b01746
ACS Appl. Mater. Interfaces 2015, 7, 12781−12788

Scheme 1. Synthetic Scheme of the DPP-based Copolymers with Different D Blocks: (a) PDDBE with (*E*)-1,2-di([2,2′-bithiophen]-5-yl)ethene (DBE) and (b) PDTTE with (*E*)-1,2-bis(6-hexylthieno[3,2-*b*]thiophen-2-yl)ethene (TTE) (see Experimental Section in the Supporting Information)

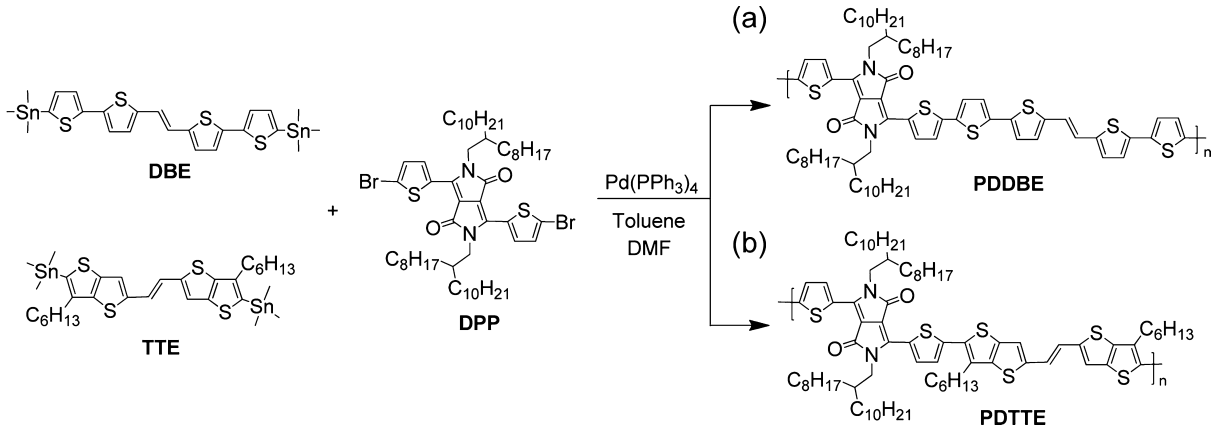

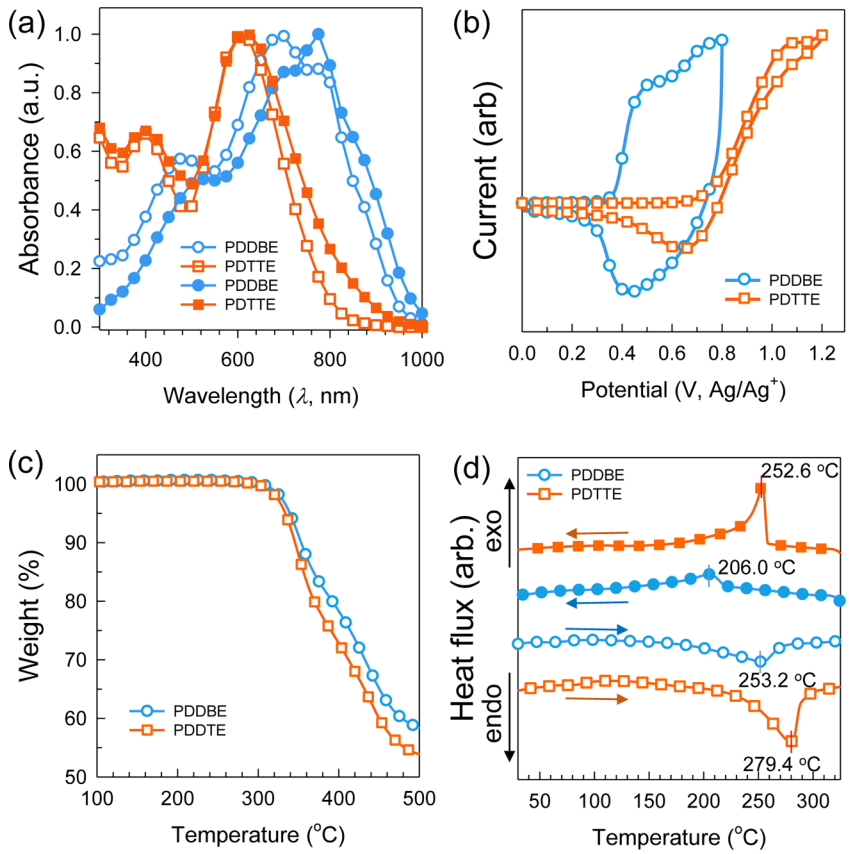

Figure 1. (a) UV−vis spectra of PDDBE and PDTTE in CF solutions (unfilled symbols) and thin films (filled symbols). (b) Cyclic voltammograms of the polymer films on a platinum electrode in 0.10 M $TBABF_4$ acetonitrile solution. (c) TGA and (d) DSC heating and cooling curves of the copolymer powders with a constant rate of 10 °C min^{-1}.

[3,4-*c*]pyrrole-1,4(2*H*,5*H*)-dione-(*E*)-1,2-bis(6-hexylthieno-[3,2-*b*]thiophen-2-yl)ethene] (PDTTE). Depending on the D block, the vinylene derivatives alternated with either bithiophene or hexyl-substituted thienothiophene yielding variations in solubility, energy state, and self-assembly of the corresponding DPP-based copolymers.

As solution-processable polymer semiconductors, the PDDBE and PDTTE copolymers developed drastically different crystal structures in spun-cast and annealed films on polymer-grafted SiO_2 dielectrics. PDDBE formed layered domains with an expectedly long π-conjugation but an intrinsically wide intermolecular π-stacking distance (referred as to $d_{(010)}$) of 3.90 Å.[20] PDTTE formed 1D nanorod-percolated agglomerates with a much shorter $d_{(010)}$ of 3.71 Å. This difference is mainly related to the alternating A−D structure of the DPP derivative with differences in D blocks. The corresponding ordered domains had a wide range of μ_{FET} from 0.01 to 1.40 cm^2 V^{-1} s^{-1} in OFETs. By using different D blocks with the DPP derivative, the corresponding copolymers had discernibly different electrical properties in solution-

DOI: 10.1021/acsami.5b01746
ACS Appl. Mater. Interfaces 2015, 7, 12781−12788

processed OFETs, specifically, a wide-range tunable characteristics of hole mobilities: 10^{-2} to 1.4 $cm^2\ V^{-1}\ s^{-1}$.

2. EXPERIMENTAL SECTION

2.1. Materials and Sample Preparation. PDDBE and PDTTE were synthesized by Stille coupling using palladium tetrakis-(triphenylphosphine) ($Pd(PPh_3)_4$) as a catalyst (see the Experimental Section in the Supporting Information). The crude copolymers were purified by successive washing with hot methanol, hexane, and acetone using a Soxhlet extractor. For dielectric surface modification of a 300 nm thick, thermally grown SiO_2 on a highly *n*-doped Si wafer, dimethylchlorosilane-terminated polystyrene (PS-$Si(CH_3)_2Cl$, M_n = 8 kDa, Polymer Source, Inc.) was dissolved in toluene and spun-cast on the substrate in a N_2-purged glovebox. The resulting films were annealed at 100 °C for 60 min, followed by rinsing with toluene and sonicating in a toluene bath for 3 min to remove unreacted PS-$Si(CH_3)_2Cl$ residue.[21,22] PDDBE and PDTTE were spun-cast onto the PS-grafted SiO_2 (referred to as gPS-SiO_2) dielectrics from 5 mg mL^{-1} solutions dissolved in chloroform (CF, T_b = 61.2 °C) or chlorobenzene (CB, T_b = 131 °C), respectively. Some as-spun films were thermally annealed at various annealing temperatures (T_A) for 60 min, based on differential scanning calorimetry (DSC) results (Figure 1d). Finally, Au electrodes were thermally evaporated through shadow-mask produced top-contact source/drain (S/D) electrodes in the OFET. The channel length (L) was 100 μm, and the width (W) was 1500 μm.

2.2. Characterization. The number-average molecular weight (M_n), weight-average molecular weight (M_w), polydispersity index (PDI, M_w/M_n), and chemical composition were determined by gel permeation chromatography (GPC, calibrated with PS standards, Waters, M590) and ^1H nuclear magnetic resonance (NMR, Varian, Mercury Plus 300 MHz spectrometer) analyses. The thermal behaviors of the copolymers were investigated with DSC (TA Instruments, Q20) and thermogravimetric analysis (TGA, TA Instruments, Q50) was conducted under a N_2 (>99.999%) atmosphere with a heating rate of 10 °C min^{-1}. Absorption spectra were measured with a UV−vis spectrophotometer (JASCO, JP/V-570).

Cyclic voltammetry (CV) was performed using an Electrochemical Analyzer (CH Instruments) system in an anhydrous acetonitrile solution containing 0.1 M tetrabutylammonium tetrafluoroborate ($TBABF_4$) as a supporting electrolyte, at a scan rate of 50 mV s^{-1}. A glassy carbon disk (~0.05 cm^2) coated with a thin polymer film, an $Ag/AgNO_3$ electrode, and a platinum wire were used as working, reference, and counter electrodes, respectively.

Atomic force microscopy (AFM, Bruker, Multimode 8) was performed for all cast films on gPS-SiO_2 substrates. The electrical characteristics of PDDBE- and PDTTE-based OFETs were measured at room temperature in a N_2-purged glovebox (H_2O < 0.1 ppm, O_2 < 0.2 ppm) using a Keithley 4200 SCS. μ_{FET} and threshold voltages (V_{th}) were calculated in a saturation regime with the equation $I_D = \mu_{FET}C_iW(2L)^{-1}(V_G - V_{th})^2$, where C_i is the capacitance of the gate dielectric. C_i for the dielectric, sandwiched between Au dots and a highly doped *n*-type Si (100) substrate, was measured with an Agilent 4284A Precision LCR meter. Two-dimensional (2D) grazing-incidence X-ray diffraction (GIXD) was performed on the semiconducting films at beamline 9A of the Pohang Light Source (PLS), Korea. The incident angle of the X-ray beam on the sample remained below 0.18°.

3. RESULTS AND DISCUSSION

Synthesized PDDBE and PDTTE copolymers had an M_n of 39 kDa and 33 kDa and a polydispersity index (PDI) of 2.1 and 1.8, respectively (Figure S1 and Table S1 in Supporting Information). The copolymers were soluble in common organic solvents such as CF, CB, and *o*-dichlorobenzene. Due to good solubility of both polymers above 5 mg in 1 mL of each solvent, all copolymer solutions in these solvents were used without any heating.

The optical properties of the polymers in CF and the solid films were investigated by UV−vis absorption analysis (Figure 1). Detailed absorption parameters, such as absorption maxima (λ_{max}), absorption edge (onset wavelength of the absorption peak, λ_{edge}), and optical band gaps (E_g^{opt}), are summarized in Table 1. The absorption spectra of the copolymer solutions differed as shown in Figure 1a. PDTTE had two major absorption bands in the 350−500 nm and 550−700 nm ranges. The absorption band in the long-λ region could be attributed to the intramolecular charge transfer (ICT) transition, while absorption in the short-λ region was related to the $\pi-\pi^*$ transition of the conjugated polymer chain. In contrast, the UV−vis spectrum of PDDBE in solution had a much broader absorption band at 350−1000 nm with a weak peak around 480 nm. The PDDBE and PDTTE solutions had a λ_{max} of 693 and 609 nm, respectively. Additionally, the UV−vis spectra of PDDBE and PDTTE spun-cast films had absorption trends similar to the corresponding solutions, except for a slight red shift. In these films, the λ_{max} was 771 nm for PDDBE and 621 nm for PDTTE, due to the enhanced intermolecular π-stacking. Longer λ_{max} and λ_{edge} of PDDBE suggest that PDDBE molecule has longer π-conjugation length and narrower band gap than those of PDTTE molecule. The E_g^{opt} of the PDDBE and PDTTE films were 1.24 and 1.41 eV, respectively, from their UV−visible absorption onsets.

Table 1. Optical and Electrochemical Properties of PDDBE and PDTTE Copolymers Synthesized in This Study

	λ_{max} (nm)					
polymer	solution[a]	film[b]	λ_{edge} (nm)	E_g^{opt} (eV)	HOMO (eV)	LUMO (eV)
PDDBE	693	771	1000	1.24	−5.07	−3.83
PDTTE	609	621	880	1.41	−5.42	−4.01

[a]Measured in dilute CF solutions. [b]Measured on quartz plates containing the corresponding spun-cast films.

The highest occupied molecular orbital (HOMO) and lowest unoccupied molecular orbital (LUMO) energy levels of PDDBE and PDTTE films were determined by CV analysis. Figure 1b shows CV curves of these polymer films. HOMO energies were determined by using the following equation: $E_{HOMO} = -e(E_{ox}^{onset} + 4.72)$ eV, where E_{ox}^{onset} is the onset oxidation potential versus Ag/Ag^+. Based on the onset oxidation potentials of PDDBE and PDTTE (i.e., 0.35 and 0.70 eV), the calculated HOMO levels were −5.07 and −5.42 eV, respectively. The LUMO levels were determined by combining the HOMO levels with E_g^{opt} values: −3.83 (for PDDBE) and −4.01 eV (for PDTTE). All energy levels of the polymers are summarized in Table 1. The PDDBE and PDTTE copolymers were expected to have intrinsically high charge transport along the backbone due to the low band-gaps of 1.24 and 1.41 eV, respectively. To better understand the electronic structures of these DPP-based copolymers, density functional theory (DFT) calculations were also performed for simplified D−A−D−A model compounds (Figure S2, Supporting Information). The molecular energy levels and the electron distribution of the HOMO/LUMO frontier orbitals were investigated. Based on the optical and theoretical results, PDDBE had shallower HOMO level than that of PDTTE due to more rigid and coplanar backbone of PDDBE.

The copolymers showed good thermal stability (Figure 1c) with 5% degradation temperatures of 339.4 °C for PDDBE and

DOI: 10.1021/acsami.5b01746
ACS Appl. Mater. Interfaces 2015, 7, 12781−12788

333.8 °C for PDTTE. Additional DSC analysis of the copolymers revealed the melting and recrystallization characteristics of typical semicrystalline polymers (Figure 1d). During the DSC heating (up to 320 °C) and cooling, the melting temperature (T_m) and crystallization temperatures (T_c) of PDDBE were determined to be 253.2 and 206.0 °C respectively. In contrast, PDTTE had a higher T_m and T_c of 279.4 and 252.6 °C, respectively. Thermal annealing temperatures (T_A) had been chosen below T_ms of the copolymers based on the DSC results.

To investigate the π-conjugated ordering of PDDBE and PDTTE copolymers in solution-cast films, 25−30 nm thick thin films were spun-cast onto gPS-SiO_2 surfaces from dilute PDDBE and PDTTE solutions in both CF and CB. Some as-spun films were further annealed at 100, 150, or 200 °C (T_A) for 60 min. Figure 2 shows typical AFM topographies of

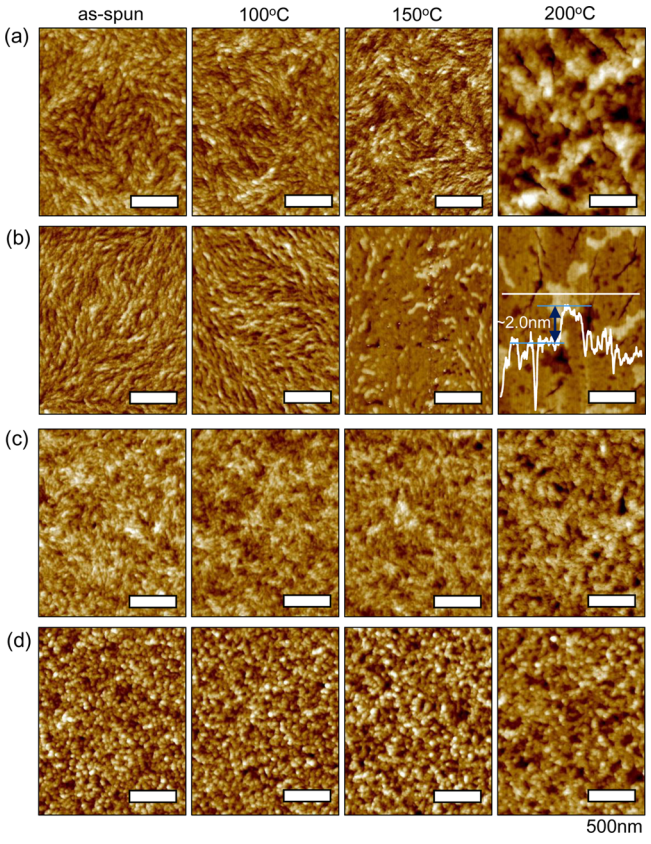

Figure 2. AFM topographies of (a and b) PDDBE and (c and d) PDTTE films spun-cast from 0.5 vol % solutions in (a and c) CF and (b and d) CB before and after annealing at different T_A.

PDDBE and PDTTE films on the gPS-SiO_2 surface, before and after annealing at various T_A. AFM of the as-spun films showed irregular nanocrystallites with a meta-structure between sphere, rod, and fibril. The structure was mainly related to insufficient crystallization time to develop extended π-conjugated crystallites during solvent evaporation (<30 s).

The as-spun PDDBE films had better ordered morphologies than did the PDTTE films. Additionally, less-volatile CB induced ordered nanostructures of both DPP-based copolymers, providing longer crystallization time than did CF (T_b = 61.2 °C). In dilute solutions, most dissolved semiconducting polymers required enough solvent-evaporation time to form extended crystal structures through both intra- and intermolecular conjugation. As shown in Figure 2a,b, a relatively slow CB evaporation induced long PDDBE nanofibrils unlike the nanorods in the quickly solidified CF system. The initial domain morphologies also considerably affected subsequent ordering development of the π-conjugated copolymer via thermal annealing. Nanofibrils in the as-spun PDDBE films evolved into multilayered domains (with a layer step of about 2.0 nm) during high-T annealing (above 150 °C; Figure 2b), while less-ordered nanorods changed into discontinuous 2D crystal flakes (Figure 2a). Like the smooth crystal layer in the 150 °C annealed film, AFM of the 200 °C annealed PDDBE film showed a layered domain, but the thermally enhanced ordering induced many geometrical defects (i.e., physical cracks with a depth of 2−11 nm), causing serious degradation of the lateral charge-carrier transport in OFET (discussed later).

In contrast, PDTTE chains were sphere- or rod-type ordered domains in the as-spun films and were hard to grow into larger grains by high-T annealing in this study. However, the ordering and percolation of the grains were enhanced as T_A increased (Figure 2c,d). The results were mainly related to less conjugation in the backbone due to the mobile TTE segment with hexyl side-chains. More coplanar conjugated polymers induce better dimensional extension of π-conjugated structures.[23,24] Hexyl moieties in TTE significantly improved the solution stability of PDTTE but seemed to interfere with the π-conjugated, assisted intra- and intermolecular chain conformation. Due to the degraded π-conjugation, the ordering structures of PDTTE were limited to nanodot or -rod domains under a rapid solvent evaporation.

In solution-processed semiconducting films, controlling the preferential domain orientation to enhance the charge-carrier transport is a key to extending π-conjugated structures with few lateral defects. Synchrotron-based 2D GIXD patterns of these PDDBE and PDTTE films on the gPS-SiO_2 substrates had intense X-ray reflections along the Q_z (out-of-plane) and Q_{xy} (in-plane) axes (Figure 3). Because the beam center and (100) peak position of the patterns were blocked with an Al beam-stopper to avoid saturating the detector with intense X-ray reflections, the actual (100) reflections along the Q_z axis for all films were higher than indicated.

As shown in Figure 3a,b, 2D GIXD patterns of the PDDBE films revealed that the orientations of the semiconducting polymer chains were drastically affected by differences in solvent evaporation rate during casting. The GIXD pattern of the as-spun PDDBE film fabricated from CF revealed large number of "face-on" chains, which had π-conjugated planes parallel to the dielectric surface, indicated by intense X-ray reflection of (010) crystal planes along the Q_z (marked as $(010)_{face\text{-}on}$ in Figure 3a and Figure S3a, Supporting Information). However, with the less-volatile CB solvent, the "edge-on" chain conformation, which forms a better conducting path, was more common than the face-on conformation. The face-on conformation was also drastically decreased in the spun-cast and further annealed films (Figure 3b and Figure S3d, Supporting Information). In particular, high-T_A annealing (above 100 °C) of the PDDBE films spun-cast from CF and CB solvents significantly improved the film ordering, while the intrinsically disordered structures remained after thermal annealing. Additionally, the layer spacing between the (100) crystal planes, $d_{(100)}$, was ~21.4 Å, and the (010) plane distance (referred as the intermolecular π-stacking distance), $d_{(010)}$, was ~3.90 Å, higher than the $d_{(010)}$ of ~3.85 Å for P3HT.[21,25]

DOI: 10.1021/acsami.5b01746
ACS Appl. Mater. Interfaces 2015, 7, 12781−12788

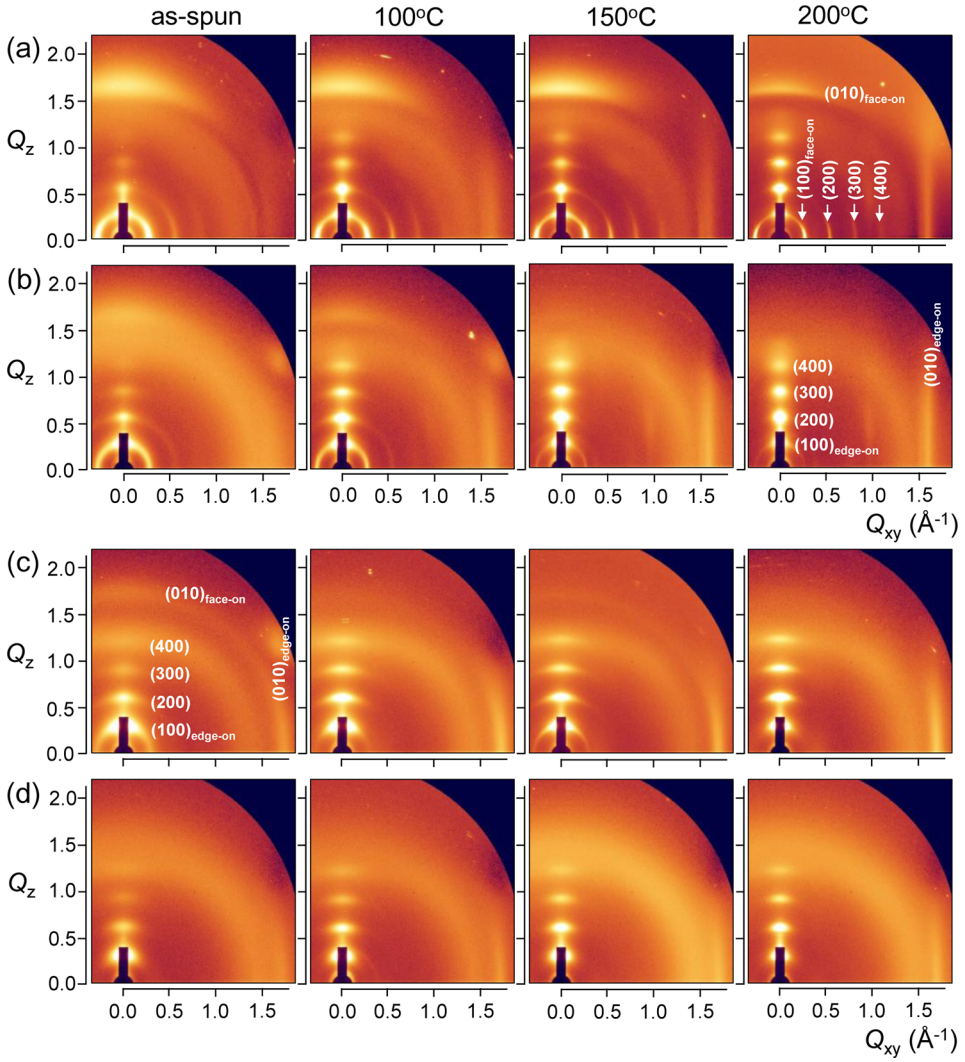

Figure 3. 2D GIXD patterns of (a, b) PDDBE and (c, d) PDTTE films spun-cast from 0.5 vol % solutions in CF (a, c) and CB (b, d), before and after annealing at different T_A.

On the basis of the 2D GIXD patterns of PDTTE films, the copolymer chains preferentially formed an edge-on chain conformation on the gPS-SiO_2 surfaces, as determined by intense $(h00)_{edge\text{-}on}$ reflections along the Q_z axis (see Figures 3c and 3d). The $d_{(100)}$ spacing was ~19.8 Å, and the $d_{(010)}$ was approximately 3.71 Å, which was much shorter than the $d_{(010)}$ of PDTTE and close to the ~3.72 Å for poly[2,5-bis(3-alkylthiophen-2-yl)thieno[3,2-*b*]thiophene] (pBTTT).[26] An increase in T_A considerably enhanced the film ordering and preferential π-orientation (Figure S4, Supporting Information).

McCulloch et al. reported that OFETs based on pBTTT films with $d_{(010)}$ of about 3.72 Å yielded the highest μ_{FET} of up to 0.7 $cm^2\ V^{-1}\ s^{-1}$.[26] The high electrical performance was mainly related to laterally μm-scale domains with few grain boundaries (GBs) compared with 1D nanogranular fibrils. Recently, to explain the unexpectedly high μ_{FET} of indacenodithiophene-based A−D copolymer films with a near-amorphous microstructure, Sirringhaus et al. suggested that a planar, torsion-free backbone conformation of these conjugated A−D copolymers could be resilient in "disorder-free" conjugated structures of each molecule for high performance OFETs.[23]

In our study, the solution-cast PDDBE and PDTTE films developed ordered structures with different characteristics. PDDBE formed layered domains with an extended π-overlap structure but a wide $d_{(010)}$ of 3.90 Å. PDTTE formed 1D nanorods with a much shorter $d_{(010)}$ of 3.71 Å. Top-contacted Au electrode OFETs containing PDDBE and PDTTE semiconducting layers (L = 100 μm and W = 1500 μm, see the insets in Figure 4) were fabricated on the bottom gPS-SiO_2 dielectrics with a C_i of 10.5 $nFcm^{-2}$. Figure 4 shows typical drain current−gate voltage (I_D−V_G) transfer curves of the OFETs with solvent type and T_A-mediated PDDBE and PDTTE films, operated at the saturation regime (drain voltage, V_D = −30 V). Table 2 lists the electrical properties of the OFETs.

All the devices had typical *p*-type transistor behavior with negligible V_G-sweep hysteresis (Figure 4 and Figure S5, Supporting Information). Additionally, it was found that the PDDBE-based OFETs could yield an ambipolar characteristics (Figure S6, Supporting Information), although PDTTE had the same strong electron-withdrawing properties of the DPP moiety.[27] The cast PDDBE film-based FETs drastically changed from 0.01 $cm^2\ V^{-1}\ s^{-1}$ to 1.40 $cm^2\ V^{-1}\ s^{-1}$. The results strongly suggest that the long-range ordering and direction of the π-

DOI: 10.1021/acsami.5b01746
ACS Appl. Mater. Interfaces 2015, 7, 12781−12788

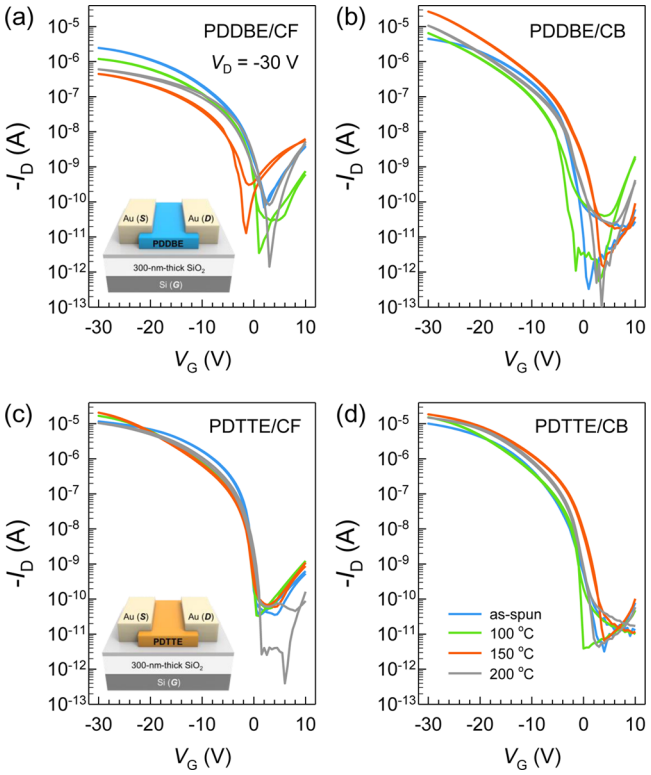

Figure 4. Typical I_D–V_G transfer curves of (a and b) PDDBE and (c and d) PDTTE films spun-cast from 0.5 vol % solutions in (a and c) CF and (b and d) CB before and after annealing at different T_A.

conjugated polymer chains played an important role in improving the charge-carrier transport.[20] The PDDBE OFETs fabricated with CF had poor μ_{FET} of 0.01–0.05 $cm^2\ V^{-1}\ s^{-1}$. Specifically, the 200 °C annealed PDDBE film showed the lowest μ_{FET} value (see Table 2), although it was highly ordered to form the largest domain. In contrast, PDDBE films spun-cast from CB solvent had a drastically better μ_{FET}. The as-cast film was 0.11 $cm^2\ V^{-1}\ s^{-1}$ in the OFET, and, after annealing at different T_A, the optimized PDDBE-based OFET had a μ_{FET} of up to 1.40 $cm^2\ V^{-1}\ s^{-1}$, threshold voltage (V_{th}) = −13.7 V, on/off current ratio $I_{ON}/I_{OFF} > 10^7$, and subthreshold swing (SS) = 0.6 V $decade^{-1}$. As confirmed by AFM and 2D GIXD analyses (Figures 2b and 3b), the layer-like domains of PDDBE with both intrinsically low band gap and the long-range ordered chain conformation were thought to overcome the wide π-stacking distance, 3.90 Å, achieving a high-performance OFET.

The as-spun PDTTE-based OFETs had μ_{FET} values of approximately 0.28 $cm^2\ V^{-1}\ s^{-1}$, which was much higher than the μ_{FET} of as-spun PDDBE-based devices, irrespective of the processing solvent (Table 2). Additional heat treatment of the as-spun films increased μ_{FET} values by about 3-fold, up to 0.72 $cm^2\ V^{-1}\ s^{-1}$ (for 150 °C annealed film) and improved V_{th} = −1.7 V and $I_{on}/I_{off} > 10^5$. However, high-T_A annealing, such as 200 °C degraded μ_{FET} to 0.25 $cm^2\ V^{-1}\ s^{-1}$ (for CF solvent) and 0.47 $cm^2\ V^{-1}\ s^{-1}$ (for CB solvent).

In semiconducting films, the percolation of small, π-conjugated grains seriously interferes with charge carrier transport along the ordered grains.[28] The as-spun and annealed PDTTE films contained short-range, ordered domains. The conjugated chains had a mostly edge-on conformation, but many grain boundaries were present due to short π-overlapped structures (Figure 2c and Figure 2d). As a result, the μ_{FET} values of the OFETs based on the PDDBE films including layer-like conjugated domains were much higher than those of the PDTTE-based OFETs.

On the basis of the structural and electrical properties of the DPP-based copolymers in OFETs, the PDDBE copolymer formed a wide π-overlap distance of approximately 3.90 Å, causing drastic degradation in charge carrier transport of a less-ordered and mixed phase film spun-cast on a gPS-treated dielectric (μ_{FET} ~10^{-2} $cm^2\ V^{-1}\ s^{-1}$), although it had a narrow HOMO–LUMO band gap of 1.26 eV (Figure 5a). However, it

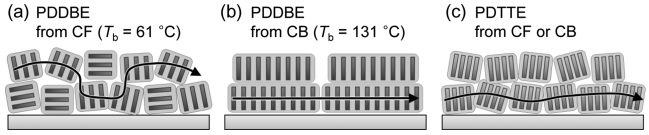

Figure 5. Schematic diagrams of π-conjugated packing and the corresponding charge-carrier transport in (a, b) PDDBE and (c) PDTTE films fabricated from different solvents. (The black arrows represent the intermolecular π-conjugated directions and the preferential charge transport paths, respectively.).

could develop 2D percolated layer-like domains via less-volatile solvent-based film processing and heat-treatment. As shown in Figure 5b, a layer-like percolation of the 2D extended crystal domains provided better charge transport along the π-conjugated molecules, yielding 1.4 $cm^2\ V^{-1}\ s^{-1}$ in an OFET.

In contrast, the PDTTE copolymer, which contained TTE as a D block, had thienothiophene-vinylene-thienothiophene backbone, forming a narrow π–π overlap of approximately 3.71 Å. The PDTTE copolymer was difficult to develop into

Table 2. Electrical Performances of PDDBE and PDTTE Films Spun-Cast from 0.5 vol % Solutions in CF and CB, before and after Annealing at Different T_A

		property							
		μ_{FET} ($cm^2\ V^{-1}\ s^{-1}$)		V_{th} (V)		SS (mV dec^{-1})		I_{ON}/I_{OFF}	
solvent	T_A (°C)	CF	CB	CF	CB	CF	CB	CF	CB
PDDBE		0.05 ± 0.003	0.11 ± 0.004	−2.8	−5.5	1,128	454	$>10^4$	~10^7
	100	0.03 ± 0.002	0.35 ± 0.015	−2.3	−15	362	461	$>10^4$	~10^7
	150	0.01 ± 0.001	1.40 ± 0.050	−1.7	−13.7	542	603	$>10^5$	$>10^7$
	200	0.01 ± 0.002	0.61 ± 0.032	3.0	−14.8	385	481	$>10^5$	~10^7
PDTTE		0.28 ± 0.013	0.28 ± 0.014	−2.5	−5.4	427	1,226	$>10^5$	$>10^6$
	100	0.48 ± 0.020	0.53 ± 0.020	−2.1	−8.7	606	370	$>10^5$	$>10^6$
	150	0.72 ± 0.031	0.47 ± 0.019	−1.7	−4.5	775	756	$>10^6$	$>10^6$
	200	0.25 ± 0.014	0.47 ± 0.023	2.2	−5.4	276	762	$>10^6$	$>10^6$

DOI: 10.1021/acsami.5b01746
ACS Appl. Mater. Interfaces 2015, 7, 12781–12788

long-range π-conjugated domains above 1 μm, due to steric hindrance by mobile hexyl side-chains (Figure 5c). The benefit of the close π-overlap distance and low band gap of PDTTE could yield high μ_{FET} values of 0.25−0.72 $cm^2\ V^{-1}\ s^{-1}$.

4. CONCLUSION

We synthesized diketopyrrolopyrrole (DPP)-based copolymers, poly[2,5-bis(2-octyldodecyl)pyrrolo[3,4-*c*]pyrrole-1,4(2*H*,5*H*)-dione-(*E*)-1,2-di([2,2′-bithiophen]-5-yl)ethene] (PDDBE) and poly[2,5-bis(2-octyldodecyl)pyrrolo[3,4-*c*]pyrrole-1,4(2*H*,5*H*)-dione-(*E*)-1,2-bis(6-hexylthieno[3,2-*b*]thiophen-2-yl)ethene] (PDTTE), by alternating a DPP acceptor block with different donor (D) blocks, including (*E*)-1,2-di([2,2′-bithiophen]-5-yl)ethene (DBE) and (*E*)-1,2-bis(6-hexylthieno[3,2-*b*]-thiophene-2-yl)ethene (TTE). As solution-processed, semiconducting channel layers in OFETs, PDDBE and PDTTE copolymers had drastically different crystal structures on polymer-grafted SiO_2 dielectrics. PDDBE preferred to form 2D layered crystallites with an extended π-conjugated structure but a wide intermolecular distance, $d_{(010)}$, of 3.90 Å, while PDTTE tended to form 1D nanorods with a much shorter $d_{(010)}$ of 3.71 Å. The corresponding crystallites yielded a wide range of field-effect mobilities (μ_{FET}) from 0.01 to 1.40 $cm^2\ V^{-1}\ s^{-1}$.

■ ASSOCIATED CONTENT

Supporting Information

Synthesis, GPC, and ^{1}H NMR spectra of PDDBE and PDTTE; 1D XRD plots of PDDBE and PDTTE films; and electrical characteristics of PDDBE- and PDTTE-based OFETs. The Supporting Information is available free of charge on the ACS Publications website at DOI: 10.1021/acsami.5b01746.

■ AUTHOR INFORMATION

Corresponding Authors

*E-mail: hcyang@inha.ac.kr. Phone: +82-32-860-7494).
*E-mail: dohoonhwang@pusan.ac.kr. Phone: +82-51-510-2232).

Author Contributions

M.J. and J.K. contributed equally.

Notes

The authors declare no competing financial interest.

■ ACKNOWLEDGMENTS

This work was supported by grants from the Center for Advanced Soft Electronics under the Global Frontier Research Program (2012M3A6A5055225) and the General Research Program (2013R1A12063963) of the Ministry of Education, Science, and Technology (MEST), Korea. Also, this work was supported by the National Research Foundation (NRF) grants funded by the Korean government (MEST) (No. 2014007318).

■ ABBREVIATIONS

OFET	organic field-effect transistor
μ_{FET}	field-effect mobility
D	donor
A	acceptor
DPP	diketopyrrolopyrrole
gPS-SiO_2	polystyrene-grafted SiO_2
M_n	number-average molecular weight
PDI	polydispersity index
λ_{max}	absorption maxima
λ_{edge}	onset wavelength of the absorption peak
E_g^{opt}	optical band gaps
E_{ox}^{onset}	onset oxidation potential
ICT	intramolecular charge transfer
HOMO	highest occupied molecular orbital
LUMO	lowest unoccupied molecular orbital
DFT	density functional theory
CV	cyclic voltammetry
DBE	(*E*)-1,2-di([2,2′-bithiophen]-5-yl)ethene
TTE	(*E*)-1,2-bis(6-hexylthieno[3,2-*b*]thiophen-2-yl)-ethene

■ REFERENCES

(1) Rogers, J. A.; Bao, Z. Printed Plastic Electronics and Paperlike Displays. *J. Polym. Sci., Part A: Polym. Chem.* **2002**, *40*, 3327−3334.
(2) Gelinck, G. H.; Huitema, H. E. A.; van Veenendaal, E.; Cantatore, E.; Schrijnemakers, L.; van der Putten, J. B. P. H.; Geuns, T. C. T.; Beenhakkers, M.; Giesbers, J. B.; Huisman, B.-H.; Meijer, E. J.; Benito, E. M.; Touwslager, F. J.; Marsman, A. W.; van Rens, B. J. E.; de Leeuw, D. M. Flexible Active-Matrix Displays and Shift Registers Based on Solution-Processed Organic Transistors. *Nat. Mater.* **2004**, *3*, 106−110.
(3) Subramanian, V.; Frechet, J. M. J.; Chang, P. C.; Huang, D. C.; Lee, J. B.; Molesa, S. E.; Murphy, A. R.; Redinger, D. R.; Volkman, S. K. Progress Toward Development of All-Printed RFID Tags: Materials, Processes, and Devices. *Proc. IEEE* **2005**, *93*, 1330−1338.
(4) Baude, P. F.; Ender, D. A.; Haase, M. A.; Kelley, T. W.; Muyres, D. V.; Theiss, S. D. Pentacene-Based Radio-Frequency Identification Circuitry. *Appl. Phys. Lett.* **2003**, *82*, 3964−3966.
(5) Bronstein, H.; Chen, Z.; Ashraf, R. S.; Zhang, W.; Du, J.; Durrant, J. R.; Tuladhar, P. S.; Song, K.; Watkins, S. E.; Geerts, Y.; Wienk, M. M.; Janssen, R. A. J.; Aothopoulos, T.; Sirringhaus, H.; Heeney, M.; McCulloch, I. Thieno[3,2-*b*]thiophene-Diketopyrrolopyrrole-Containing Polymers for High-Performance Organic Field-Effect Transistors and Organic Photovoltaic Devices. *J. Am. Chem. Soc.* **2011**, *133*, 3272−3275.
(6) Qu, S. Y.; Tian, H. Diketopyrrolopyrrole (DPP)-Based Materials for Organic Photovoltaics. *Chem. Commun.* **2012**, *48*, 3039−3051.
(7) Someya, T.; Dodabalapur, A.; Huang, J.; See, K. C.; Katz, H. E. Chemical and Physical Sensing by Organic Field-Effect Transistors and Related Devices. *Adv. Mater.* **2010**, *22*, 3799−3811.
(8) Berggren, M.; Richter-Dahlfors, A. Organic Bioelectronics. *Adv. Mater.* **2007**, *19*, 3201−3213.
(9) Klauk, H. Organic Thin-Films Transistors. *Chem. Soc. Rev.* **2010**, *39*, 2643−2666.
(10) Kang, I.; Yun, H. J.; Chung, D. S.; Kwon, S. K.; Kim, Y. H. Record High Hole Mobility in Polymer Semiconductors via Side-Chain Engineering. *J. Am. Chem. Soc.* **2013**, *135*, 14896−14899.
(11) Yuan, Y. B.; Giri, G.; Ayzner, A. L.; Zoombelt, A. P.; Mannsfeld, S. C. B.; Chen, J. H.; Nordlund, D.; Toney, M. F.; Huang, J. S.; Bao, Z. N. Ultra-High Mobility Transparent Organic Thin Films Transistors Grown by an Off-Centre Spin-Coating Method. *Nat. Commun.* **2014**, *5*, 3005.
(12) Diao, Y.; Tee, B. C.-K.; Giri, G.; Xu, J.; Kim, D. H.; Becerril, H. A.; Stoltenberg, R. M.; Lee, T. H.; Xue, G.; Mannsfeld, S. C. B.; Bao, Z. Solution Coating of Large-Area Organic Semiconductor Thin Films with Aligned Single-Crystalline Domains. *Nat. Mater.* **2013**, *12*, 665−671.
(13) Yang, H.; Shin, T. J.; Yang, L.; Cho, K.; Ryu, C. Y.; Bao, Z. N. Effect of Mesoscale Crystalline Structures on the Field-Effect Mobility of Regioregular Poly(3-hexyl thiophene) in Thin-Films Transistors. *Adv. Funct. Mater.* **2005**, *15*, 671−676.
(14) Wang, C. C.; Jimison, L. H.; Goris, L.; McCulloch, I.; Heeney, M.; Ziegler, A.; Salleo, A. Microstructural Origin of High Mobility in High-Performance Poly(thienothiophene) Thin-Film Transistors. *Adv. Mater.* **2010**, *22*, 697−701.

DOI: 10.1021/acsami.5b01746
ACS Appl. Mater. Interfaces 2015, 7, 12781−12788

(15) Liu, J. Y.; Zhang, R.; Sauve, G.; Kowalewski, T.; McCullough, R. D. Highly Disordered Polymer Field Effect Transistors: *N*-Alkyl Dithieno[3,2-*b*:2′,3′-*d*]pyrrole-Based Copolymers with Surprisingly High Charge Carrier Mobilities. *J. Am. Chem. Soc.* **2008**, *130*, 13167−13176.
(16) Zhan, X. W.; Tan, Z. A.; Domercq, B.; An, Z. S.; Zhang, X.; Barlow, S.; Li, Y. F.; Zhu, D. B.; Kippelen, B.; Marder, S. R. A High Mobility Electron-Transport Polymer with Broad Absorption and Its Use in Field-Effect Transistors and All-Polymer Solar Cells. *J. Am. Chem. Soc.* **2007**, *129*, 7246−7247.
(17) Bijleveld, J. C.; Gevaerts, V. S.; Di Nuzzo, D.; Turbiez, M.; Mathijssen, S. G. J.; de Leeuw, D. M.; Wienk, M. M.; Janssen, R. A. J. Efficient Solar Cells Based on an Easily Accessible Diketopyrrolopyrrole Polymer. *Adv. Mater.* **2010**, *22*, E242−E246.
(18) Liu, S. Y.; Shi, M. M.; Huang, J. C.; Jin, Z. N.; Hu, X. L.; Pan, J. Y.; Li, H. Y.; Jen, A. K. Y.; Chen, H. Z. C−H Activation: Making Diketopyrrolopyrrole Derivative Easily Accessible. *J. Mater. Chem. A* **2013**, *1*, 2795−2805.
(19) Kanimozhi, C.; Yaacobi-Gross, N.; Chou, K. W.; Amassian, A.; Anthopoulos, T. D.; Patil, S. Diketopyrrolopyrrole-Diketopyrrolopyrrole-Based Conjugated Copolymer for High-Mobility Organic Field-Effect Transistors. *J. Am. Chem. Soc.* **2012**, *134*, 16532−16535.
(20) Rivnay, J.; Toney, M. F.; Zheng, Y.; Kauvar, I. V.; Chen, Z.; Wagner, V.; Facchtti, A.; Salleo, A. Unconventional Face-On Texture and Exceptional In-Plane Order of a High Mobility *n*-Type Polymer. *Adv. Mater.* **2010**, *22*, 4359−4363.
(21) Kim, S. H.; Jang, M.; Yang, H.; Anthony, J. E.; Park, C. E. Physicochemically Stable Polymer-Coupled Oxide Dielectrics for Multipurpose Organic Electronic Applications. *Adv. Funct. Mater.* **2011**, *21*, 2198−2207.
(22) Lee, S.; Jang, M.; Yang, H. Optimized Grafting Density of End-Functionalized Polymers to Polar Dielectric Surfaces for Solution-Processed Organic Field-Effect Transistors. *ACS Appl. Mater. Interfaces* **2014**, *6*, 20444−20451.
(23) Venkateshvaran, D.; Nikolka, M.; Sadhanala, A.; Lemaur, V.; Zelazny, M.; Kepa, M.; Hurhangee, M.; Kronemeijer, A. J.; Pecunia, V.; Nasrallah, I.; Romanov, I.; Broch, K.; McCulloch, I.; Emin, D.; Olivier, Y.; Cornil, J.; Beljonne, D.; Sirringhaus, H. Approaching Disorder-Free Transport in High-Mobility Conjugated Polymers. *Nature* **2014**, *515*, 384−388.
(24) Lee, J. S.; Son, S. K.; Song, S.; Kim, H.; Lee, D. R.; Kim, K.; Ko, M. J.; Choi, D. H.; Kim, B.; Cho, J. H. Importance of Solubilizing Group and Backbone Planarity in Low Band Gap Polymers for High Performance Ambipolar Field-Effect Transistors. *Chem. Mater.* **2012**, *24*, 1316−1323.
(25) Niklas, J.; Mardis, K. L.; Banks, B. P.; Grooms, G. M.; Sperlich, A.; Dyakonov, V.; Beaupre, S.; Leclerc, M.; Xu, T.; Yu, L.; Poluektov, O. G. Highly-Efficient Charge Separation and Polaron Delocalization in Polymer-Fullerene Bulk-Heterojunctions: A Comparative Multi-Frequency EPR and DFT Study. *Phys. Chem. Chem. Phys.* **2013**, *15*, 9562−9574.
(26) McCulloch, I.; Heeney, M.; Bailey, C.; Genevicius, K.; MacDonald, I.; Shkunov, M.; Sparrowe, D.; Tierney, S.; Wagner, R.; Zhang, W.; Chabinyc, M. L.; Kline, R. J.; McGehee, M. D.; Toney, M. F. Liquid-Crystalline Semiconducting Polymers with High Charge-Carrier Mobility. *Nat. Mater.* **2006**, *5*, 328−333.
(27) Lin, H. W.; Lee, W. Y.; Chen, W. C. Selenophene-DPP Donor-Acceptor Conjugated Polymer for High Performance Ambipolar Field Effect Transistor and Nonvolatile Memory Applications. *J. Mater. Chem.* **2012**, *22*, 2120−2128.
(28) Jang, M.; Park, J. H.; Im, S.; Kim, S. H.; Yang, H. Critical Factors to Achieve Low Voltage- and Capacitance-Based Organic Field-Effect Transistors. *Adv. Mater.* **2014**, *26*, 288−292.

DOI: 10.1021/acsami.5b01746
ACS Appl. Mater. Interfaces 2015, 7, 12781−12788